

Review

A Review on Visible Light Active Perovskite-Based Photocatalysts

Pushkar Kanhere ^{1,2,*} and **Zhong Chen** ^{1,2,*}

¹ Energy Research Institute @ NTU, 1 CleanTech Loop, Clean Tech One, Singapore 637141, Singapore

² School of Materials Science and Engineering, Nanyang Technological University, 50 Nanyang Avenue, Singapore 639798, Singapore

* Authors to whom correspondence should be addressed; E-Mails: pkanhere@gmail.com (P.K.); ASZChen@ntu.edu.sg (Z.C.); Tel.: +65-67904256 (Z.C.); Fax: +65-67909081 (Z.C.).

External Editor: Pierre Pichat

Received: 25 September 2014; in revised form: 13 November 2014 / Accepted: 16 November 2014 /

Published: 1 December 2014

Abstract: Perovskite-based photocatalysts are of significant interest in the field of photocatalysis. To date, several perovskite material systems have been developed and their applications in visible light photocatalysis studied. This article provides a review of the visible light ($\lambda > 400$ nm) active perovskite-based photocatalyst systems. The materials systems are classified by the B site cations and their crystal structure, optical properties, electronic structure, and photocatalytic performance are reviewed in detail. Titanates, tantalates, niobates, vanadates, and ferrites form important photocatalysts which show promise in visible light-driven photoreactions. Along with simple perovskite (ABO_3) structures, development of double/complex perovskites that are active under visible light is also reviewed. Various strategies employed for enhancing the photocatalytic performance have been discussed, emphasizing the specific advantages and challenges offered by perovskite-based photocatalysts. This review provides a broad overview of the perovskite photocatalysts, summarizing the current state of the work and offering useful insights for their future development.

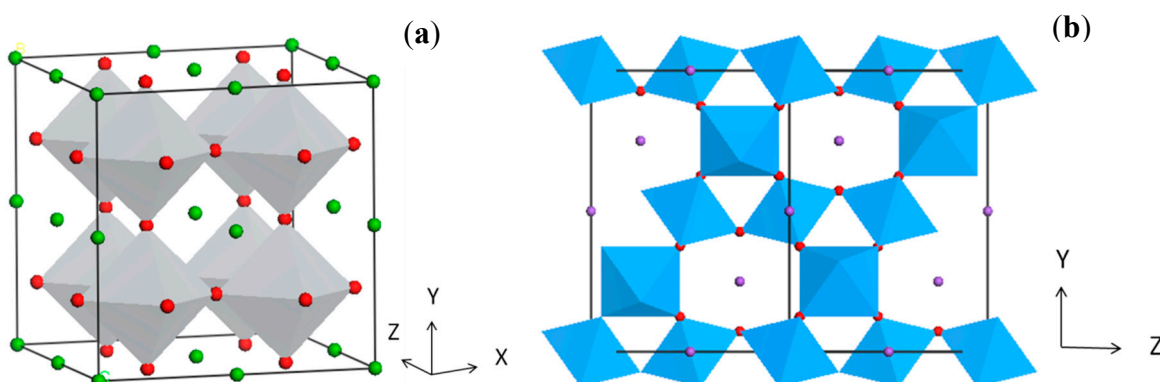
Keywords: perovskite; photocatalysis; visible light active; water splitting; doping

1. Introduction

Photocatalysis has long been studied for clean energy and environmental applications. Over the past two decades, the number of applications based on photocatalysis has increased sharply, while a wide range of materials systems have been developed [1–4]. Photocatalysis has been of particular interest in the production of hydrogen from water using solar energy [5]. Further, conversion of CO₂ to hydrocarbons (fuels) is also of significant interest, as it is a solution to reduce CO₂ emissions across the globe [6,7]. Apart from the clean energy generation, photocatalysis has several promising applications in the environmental field. Some of the applications include degradation of volatile organic compounds (VOC) for water treatment [8], germicide and antimicrobial action [9–11], de-coloration of industrial dyes [12–14], nitrogen fixation in agriculture [15], and removal of NO_x/SO_x air pollutants [16–19]. These applications have driven the development of variety of materials systems which are suitable for specific applications. Although TiO₂-based materials are the most studied for photocatalytic applications, ternary and other complex oxide systems have been increasingly explored as photocatalysts. Among the various classes of materials studied, perovskites-based photocatalysts have unique photophysical properties and offer distinct advantages.

Perovskites are the class of compounds presenting the general formula ABO₃. Generally, in this crystal structure, the A site is occupied by the larger cation, while the B site is occupied by the smaller cation. Perovskites are one of the most important families of materials exhibiting properties suitable for numerous technological applications [20]. Perovskite compounds such as PbZrO₃, BaTiO₃, PbTiO₃ are most commonly used piezoelectric compounds [21]. BiFeO₃ thin films show multiferroic behavior [22], while compounds such as SrTiO₃ have shown excellent photocatalytic properties [23,24]. The origin of such properties lies in the crystal structure of perovskites. The perovskite crystal structure has corner connected BO₆ octahedra and 12 oxygen coordinated A cations, located in between the eight BO₆ octahedra (Figure 1). The perfect structure of the octahedral connection results in a cubic lattice. However, depending on the ionic radii and electronegativity of the A and B site cations, tilting of the octahedra takes place, which gives rise to lower symmetry structures. As seen from the crystal structure, B site cations are strongly bonded with the oxygen (or any other anion) while, A site cations have relatively weaker interactions with oxygen. Depending on the type of the cations occupying the lattice sites, these interactions could be altered to yield the different perovskite crystal geometries.

Figure 1. Crystal structure of simple Perovskite, (a) BaTiO₃ and (b) double perovskite Na₂Ta₂O₆ (red: oxygen, green and purple: A site cation, grey and blue: BO₆ octahedra).



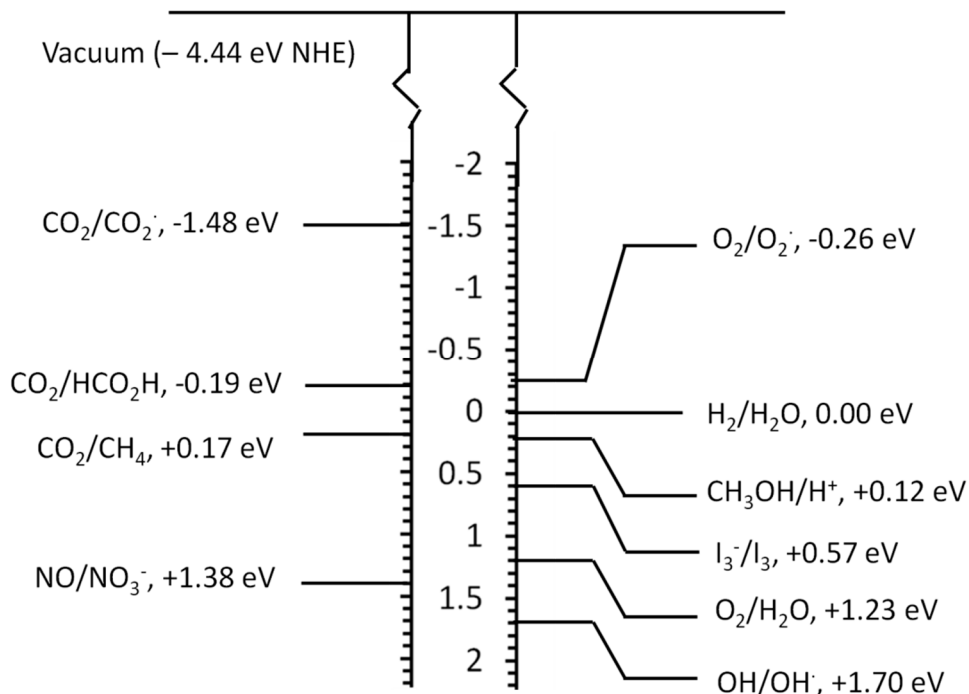
For example, different degrees of tilting of the octahedra give rise to different crystal fields, which result in different electronic and optical properties. The degrees of tilting may affect the band structure, electron and hole transport properties, photoluminescence, and dielectric behavior [25,26]. From the point of view of photocatalysis, perovskite structures may offer significant advantages over the corresponding binary oxides for several reasons. Firstly, perovskites could offer favorable band edge potentials which allow various photoinduced reactions. For example, as compared to the binary oxides, several perovskites have sufficiently cathodic conduction band (CB) energies for hydrogen evolution. Secondly, A and B site cations in the lattice give a broader scope to design and alter the band structure as well as other photophysical properties. In the case of double perovskites such as $A_2B_2O_6$, stoichiometric occupation of two cations at the B site is known to be beneficial for visible light photocatalysis. Thirdly, some studies have shown that it is possible to combine the effects such as ferroelectricity or piezoelectricity with the photocatalytic effect to benefit the photocatalytic activity.

Perovskite photocatalysts have been studied to a great extent because of their promise for being visible light active. A review of the present work on the visible light driven perovskite photocatalysts is essential to provide a broad overview and possible future directions. Shi *et al.* reported a general review of perovskite photocatalysts active under UV and visible light [27]. The current review article is focused on visible light active perovskite compounds. We emphasize the strategies used to develop or enhance the visible light absorption and subsequent photocatalytic activities. Further, we attempt to shed some light on the underlying principles specific to the perovskite crystal structure which play an important role in the photocatalytic activity, suggesting potential areas in the field where further work is needed. The first section of the article discusses the mechanism and thermodynamics of some of the most important photocatalytic reactions, while the later section reviews the material systems in detail. In the current review, perovskites are broadly divided into simple (ABO_3 type) perovskites and complex perovskites (double, layered, *etc.*).

2. Overview of Photocatalytic Reactions

Photocatalysis is a process that utilizes the energy input from incident radiation and the catalytic properties of the surface of a material to carry out and/or accelerate certain chemical reactions. To date, numerous chemical reactions have been studied, which are potentially useful in energy generation and environmental cleaning applications. Photocatalysis is known to be able to produce thermodynamically uphill reactions, which otherwise need intense energy inputs in terms of high temperature (or pressure). Understanding the mechanism of photocatalytic reactions is critically important to design and develop new photocatalytic materials. In this section, a brief review of mechanism and thermodynamics of most common photocatalytic reactions is presented. Figure 2 shows the reduction and oxidation levels of some of the common photocatalytic reactions with reference to vacuum and the normal hydrogen electrode (NHE). It is noted that these values provide an insight only on the thermodynamic feasibility of the reaction. It is seen that for the reduction reaction, the energy of the (photoexcited) electron should be higher (on the absolute vacuum scale) than the redox level. Therefore the CB potential of the photocatalyst should be located at a higher energy value than the reduction reaction of interest.

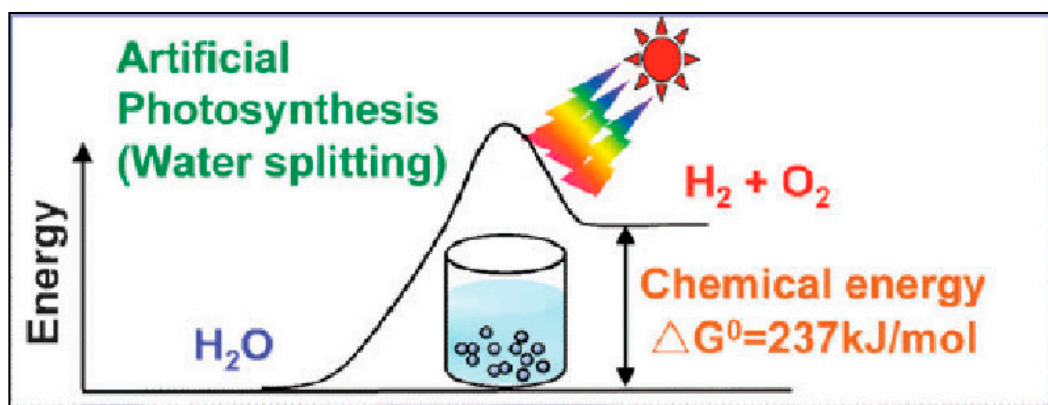
Figure 2. Energy levels of some of the important photocatalytic reactions with respect to NHE at pH = 0 [28].



2.1. Photocatalytic Water Splitting

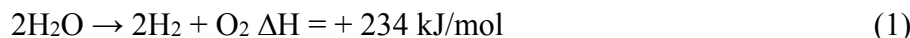
One of the most studied reactions is the direct splitting of water into hydrogen and oxygen. Figure 3 shows the schematics of the water splitting reaction according to the 4-photon model [29].

Figure 3. Band diagram and schematics of water splitting reaction over a photocatalyst surface [30].



In the water splitting reaction, upon the radiation of photon with suitable wavelength, photoexcited pairs of electrons and holes are generated within a photocatalyst. Typically, electron-hole separation takes place, due to surface charge or co-catalyst loading. Direct oxidation of water molecules, chemisorbed on the surface of the photocatalyst (or co-catalyst) occurs, by the interaction of water molecule and hole in the valence band (VB) of the photocatalyst. This reaction results in liberation of

an oxygen molecule and 4-protons. The protons then migrate to the sites of photoexcited electrons to form hydrogen molecules (Equations (1)–(3)).

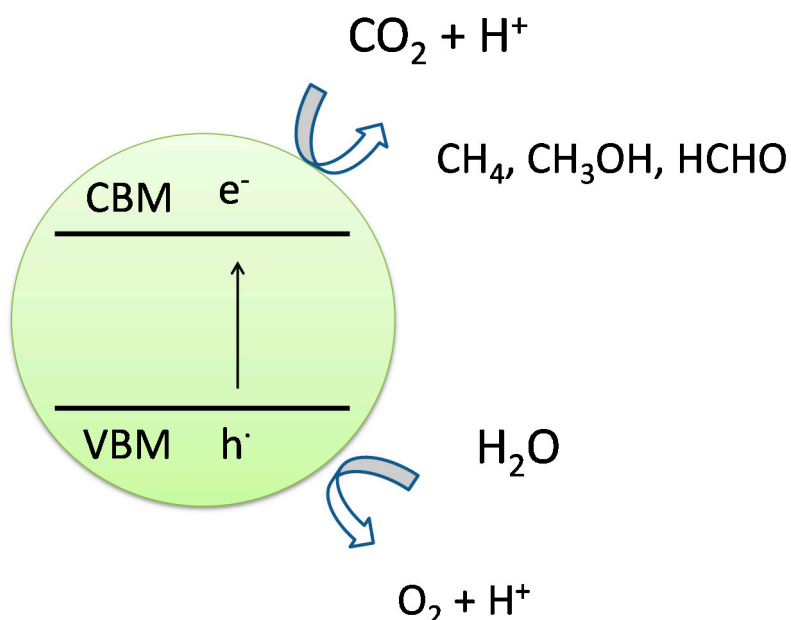


Evolution of hydrogen and oxygen using sunlight is considered as one of the most promising ways to generate hydrogen as a clean and renewable fuel. Like the water molecule, other molecules also undergo decomposition by the process of photocatalysis.

2.2. Photooxidation of Organic Molecules

Several organic compounds undergo photooxidation reactions, where a direct oxidation via photogenerated holes occurs or an indirect oxidation via hydroxyl ions takes place [31]. The degradation of organic molecules also takes place by reactive oxygen species (Figure 4). Organic dyes, aliphatics and aromatic hydrocarbons, and organic acids can be mineralized to CO_2 and H_2O by photocatalytic processes. Like organic compounds, hydroxyl ions and reactive oxygen species (ROS) are known to inactivate microorganisms by degrading their cell walls [10,32]. The photocatalytic inactivation of microbes is effective in antimicrobial, antifungal and antiviral applications. A later section reviews certain silver- and bismuth-based perovskites which display particularly efficient antimicrobial action under visible light.

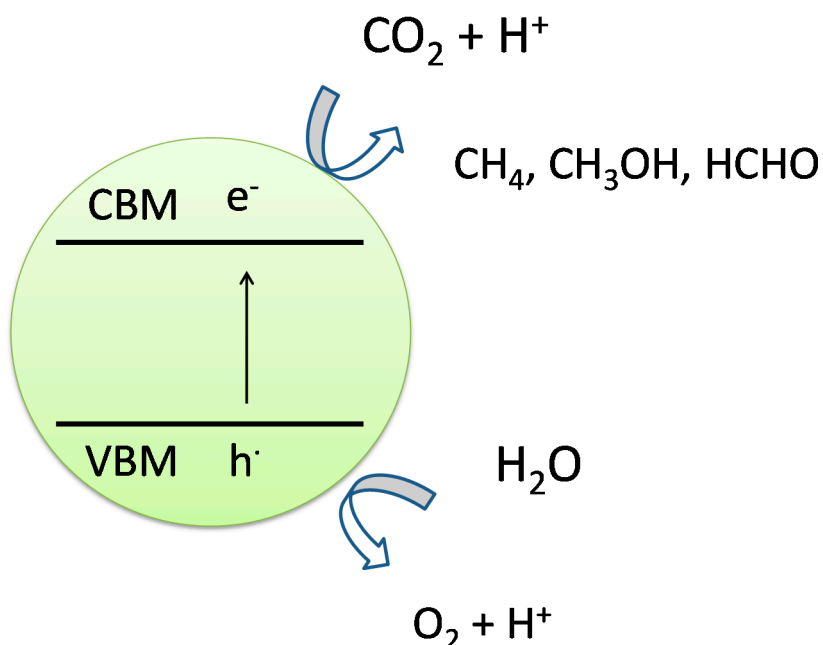
Figure 4. Band diagram and schematics of degradation of organic compounds over a photocatalyst surface [12,33].



2.3. Photocatalytic Conversion of CO₂ to Fuels

CO₂, with a standard enthalpy of formation of $-393.5 \text{ kJ}\cdot\text{mol}^{-1}$ at 298 K, is one of the most stable molecules. With appropriate adsorption and photocatalytic processes, reduction of CO₂ in presence of water could be performed to produce hydrocarbons (Figure 5). Possible chemical reactions of adsorbed CO₂ and protons are presented by the following equations (Equations (4)–(7)). It could be seen that different number of protons in the reactants, results in different hydrocarbons as products.

Figure 5. Schematics of CO₂ photoreduction reaction over a photocatalyst surface [34].

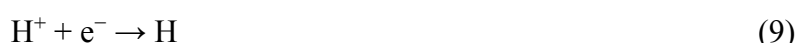


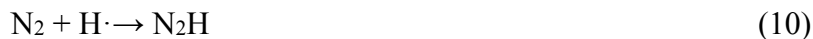
Among these reactions, the reaction with eight protons converting CO₂ to methane is of significant interest. The photocatalytic reduction of CO₂ in the presence of water is a complex reaction and the photocatalyst must possess enough band potential for proton generation:



2.4. Photocatalytic Nitrogen Fixation

Like CO₂ reduction, atmospheric nitrogen could be reduced to ammonia or nitrates by the photocatalytic processes. The mechanism of nitrogen reduction is similar to that of CO₂, where chemically adsorbed nitrogen molecules react catalytically with protons and form compounds of nitrogen and hydrogen (Equations (8)–(10)):





The photocatalytic reduction of nitrogen is extremely useful in nitrogen photofixation processes for agricultural applications [35–37]. Although the process of photocatalytic nitrogen fixation is promising, efforts in this area have been severely limited. It is noted that the mechanism of the photocatalytic processes presented above is a simplified understanding, while the photocatalytic processes are complex in nature.

It is known that a given chemical reaction has a specific photooxidation or photoreduction level (potential) and thus the band potentials of the photocatalyst must satisfy the thermodynamic conditions. Intrinsic properties such as band gap (optical absorption) and band edge potentials determine the thermodynamic feasibility of photoinduced reactions under light irradiation. Apart from the basic conditions, there are several factors which affect the photocatalytic performance of the material system under consideration. Properties such as electron and hole effective mass, exciton lifetime and diffusion length, exciton binding energy affect the electron-hole separation and transport within the lattice. These properties are known to strongly influence the performance (kinetics/efficiency) of the photocatalytic reactions. Defects in the lattice, defect-induced energy states, localization of electrons on specific defect sites could determine the fate of the photoexcited electron-hole pair. Finally, the electron transfer across semiconductor-electrolyte interface is significantly affected by surface states, surface band structure (depletion region induced electric field), and band bending. Such electronic properties of materials could be altered to suit specific photocatalytic applications. To date, numerous material systems have been evolved through systematic efforts of understanding and improving the electronic properties of materials. Among these materials perovskites have shown excellent promise for efficient photocatalysis under visible light irradiation, on account of their unique crystal structure and electronic properties. The perovskite crystal structure offers an excellent framework to tune the band gap values to enable visible light absorption and band edge potentials to suit the needs of specific photocatalytic reactions. Further, lattice distortion in perovskite compounds strongly influences the separation of photogenerated charge carriers. The following sections present some groups of materials that have shown visible light activity.

3. Simple Perovskites with Visible Light Response

3.1. Titanate Perovskites

Titanate perovskites have been studied for photocatalytic applications for a long time. Most of the titanate perovskites have band gap energy (E_g) value more than 3.0 eV, however they show excellent photocatalytic properties under UV radiation [1]. Using these titanates as host materials, doping is widely used to alter the optical properties and induce visible light absorption. TiO_2 (anatase) has a band gap of 3.2–3.4 eV and its CB potential is -0.3 to -0.6 eV above the water reduction level [38]. Certain perovskite titanates have CB energies more negative than TiO_2 , making them more suitable candidates for hydrogen generation. Titanates also offer good photostability and corrosion resistance in aqueous solutions. In this section, a detailed review of MTiO_3 ($\text{M} = \text{Sr}, \text{Ba}, \text{Ca}, \text{Mn}, \text{Co}, \text{Fe}, \text{Pb}, \text{Cd}, \text{Ni}$) systems is presented. Figure 6 gives an overview of elements that form perovskite titanates.

Figure 6. Overview of elements forming perovskite titanates useful for visible light photocatalysis.

1	H hydrogen 1.008	2	II A	13	III A	14	IV A	15	V A	16	VI A	17	VII A	2																																																																													
3	Li lithium 6.941	4	Be beryllium 9.012	5	Cr chromium 52.00	6	Mn manganese 54.94	7	Fe iron 55.85	8	Co cobalt 58.93	9	Ni nickel 58.69	10	Cu copper 63.55	11	Zn zinc 65.41	12	II B																																																																								
11	Na sodium 22.99	12	Mg magnesium 24.31	13	Sc scandium 44.96	14	Ti titanium 47.87	15	V vanadium 50.94	16	Mn manganese 54.94	17	Fe iron 55.85	18	Co cobalt 58.93	19	Ni nickel 58.69	20	Cu copper 63.55	21	Zn zinc 65.41																																																																						
19	K potassium 39.10	20	Ca calcium 40.08	21	Sc scandium 44.96	22	Ti titanium 47.87	23	V vanadium 50.94	24	Cr chromium 52.00	25	Mn manganese 54.94	26	Fe iron 55.85	27	Co cobalt 58.93	28	Ni nickel 58.69	29	Cu copper 63.55	30	Zn zinc 65.41																																																																				
37	Rb rubidium 85.47	38	Sr strontium 87.62	39	Y yttrium 88.91	40	Zr zirconium 91.22	41	Nb niobium 92.91	42	Mo molybdenum 95.94	43	Tc technetium 98	44	Ru ruthenium 101.1	45	Rh rhodium 102.9	46	Pd palladium 106.4	47	Ag silver 107.9	48	Cd cadmium 112.4	49	Ga gallium 69.72	50	Ge germanium 72.64	51	As arsenic 74.92	52	Se selenium 78.96	53	Br bromine 79.90	54	Kr krypton 83.80																																																								
55	Cs cesium 132.9	56	Ba barium 137.3	71	Lu lutetium 175.0	72	Hf hafnium 178.5	73	Ta tantalum 180.9	74	W tungsten 183.8	75	Re rhenium 186.2	76	Os osmium 190.2	77	Ir iridium 192.2	78	Pt platinum 195.1	79	Au gold 197.0	80	Hg mercury 200.6	81	Tl thallium 204.4	82	Bi bismuth 207.2	83	Po polonium 209.0	84	At astatine 210	85	Rn radon 222	86																																																									
87	Fr francium 223	88	Ra radium 226	#	Lr lawrencium 262	#	Rf rutherfordium 261	#	Db dubnium 262	#	Sg seaborgium 266	#	Bh bohrium 264	#	Hs hassium 277	#	Mt meitnerium 268	#	Ds darmstadtium 281	#	Rg roentgenium 272	#	Cn copernicium 285	#	Uut ununtrium 284	F1 florium 289	Up ununpentium 288	Lv livornium 292	Uus ununseptium 293	Uuo ununoctium 294	2	He helium 4.003																																																											
2p	5	B boron 10.81	6	C carbon 12.01	7	N nitrogen 14.01	8	O oxygen 16.00	9	F fluorine 19.00	10	Ne neon 20.18	3p	13	Al aluminum 26.98	14	Si silicon 28.09	15	P phosphorus 30.97	16	S sulfur 32.07	17	Cl chlorine 35.45	18	Ar argon 39.95	31	32	Ga gallium 69.72	33	Ge germanium 72.64	34	As arsenic 74.92	35	Se selenium 78.96	36	Br bromine 79.90	37	In indium 114.8	38	Sn tin 118.7	39	Sb antimony 121.8	40	Te tellurium 127.6	41	I iodine 126.9	42	Xe xenon 131.3	49	Tl thallium 204.4	50	Bi bismuth 207.2	51	Po polonium 209.0	52	At astatine 210	53	Rn radon 222	54	55	56	57	58	59	60	61	62	63	64	65	66	67	68	69	70	71	72	73	74	75	76	77	78	79	80	81	82	83	84	85	86

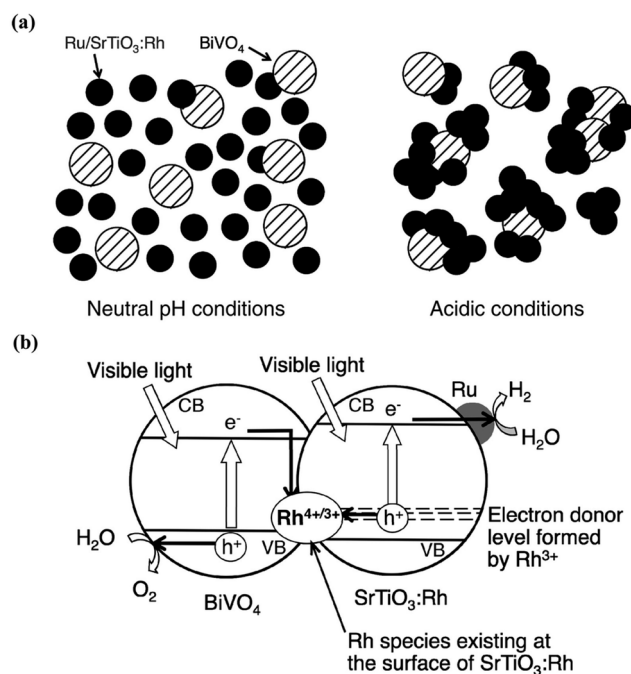
3.1.1. SrTiO₃

SrTiO_3 is a simple cubic ($\text{Pm}3\text{m}$, $a = 3.9 \text{ \AA}$) perovskite with an indirect band gap of 3.25 eV [39]. When loaded with a co-catalyst such as Rh or NiO_x , SrTiO_3 shows stoichiometric water splitting under UV radiation [40] and has been studied extensively for developing visible light water splitting catalysts. Doping of the Ti site with Mn, Ru, Rh, and Ir was of significant interest in early days [41]. It is found that these dopants induce mid-gap states in the band gap allowing visible light absorption [42]. Mn and Ru doping are found useful for O_2 evolution, while dopants like Ru, Rh, and Ir are suitable for H_2 evolution [41]. Rh-doped SrTiO_3 thin films also shows cathodic photocurrent from overall water splitting under visible light, where 7% Rh doped SrTiO_3 showed 0.18% incident photo-to-electron conversion efficiency (IPEC) under 420 nm irradiation [43]. Using Rh-doped SrTiO_3 as a H_2 evolving photocatalyst, various Z scheme systems have been developed. In a significant demonstration, a novel electron mediator $[\text{Co}(\text{bpy})_3]^{3+/2+}$ was used for Rh-doped SrTiO_3 with BiVO_4 photocatalyst. Such a system showed a solar energy conversion efficiency of 0.06% under daylight [44]. Efforts in Z scheme photocatalysis have also been targeted towards eliminating the need for electron mediators by preparing composite photocatalysts. In such systems, electrons from an O_2 evolving photocatalyst recombine with holes from a H_2 evolving photocatalyst at the interface of the composite. The quality of the interface and the band alignment of the two semiconductors are important factors for the successful realization of mediator-free type Z schemes.

Rh-doped SrTiO₃ was combined with several O₂-evolving photocatalysts such as BiVO₄, AgNbO₃, Bi₂MoO₆, WO₃, or Cr/Sb-doped TiO₂ [45]. In those experiments the authors found that agglomeration of the photocatalyst particles occur under acidic conditions, which results in Z scheme photocatalysis. A combination of Rh-doped SrTiO₃ and BiVO₄ resulted in the best yield [45]. A schematic of microstructure and mechanism of water splitting of an agglomerated Z scheme photocatalyst is shown in Figure 7. In a recent effort, a composite of 1% Rh-doped SrTiO₃ loaded with 0.7% Ru and BiVO₄ was successfully prepared. Such a composite showed a stoichiometric water splitting reaction (pH 7)

with quantum yield (QY) of 1.6% at 420 nm [23]. These studies successfully establish the feasibility of the “Z scheme” photocatalysis for candidates such as Rh-doped SrTiO₃ under visible light.

Figure 7. (a) Schematic microstructure and **(b)** band diagram of Z scheme photocatalysis using Rh-doped SrTiO₃ [45].



Further, the water splitting efficiency is dependent on the synthesis method used for Rh-doped SrTiO₃ [46]. The use of excess Sr in hydrothermal and complex polymerization methods proved useful for improving the apparent yield to 4.2% under 420 nm radiation [46]. Apart from mono-doping, co-doping has been employed in SrTiO₃ to pursue visible light driven photocatalysis. Co-doping of Sb (1%) and Rh (0.5%) was found useful for visible light photocatalysis and estimated H₂ and O₂ evolution rates for 1 m² surface area were 26 mL·h⁻¹ and 13 mL·h⁻¹, respectively [47]. Further, a composite system was prepared from co-doped La-Cr in SrTiO₃ and co-doped La-Cr Sr₂TiO₄ which showed visible light driven H₂ evolution (24 μmol·h⁻¹·g⁻¹) [48]. Composite preparation led to heterojunctions between doped phases and produced a synergistic effect for hydrogen evolution. Further, a solid solution of AgNbO₃ and SrTiO₃ was discovered to be a visible light active photocatalyst [49]. (AgNbO₃)_{0.75}(SrTiO₃)_{0.25} showed promising performance for O₂ evolution and isopropanol (IPA) degradation under visible light.

Several efforts have been made to understand and design SrTiO₃-based photocatalysts. Particularly DFT-based band structure calculations provide useful insights into the electronic structure and its correlation with photocatalytic activity. It is shown that Rh doping in SrTiO₃ produces band-like states above the valence band maximum (VBM) which are responsible for the visible light absorption. The proximity of dopant-induced states to VBM helps efficient replenishment of electrons and suppresses electron trapping from CB [42]. Theoretical calculations indicate that a TiO₂-terminated SrTiO₃ surface with defects such as O and Sr vacancies would alter its electronic structure and induce visible light absorption peaking around 420 nm [50]. Such strategies could be useful in the development of low dimensional materials. Further, theoretical work on doped SrTiO₃ compounds show that certain

dopants such as La strongly lower the effective mass of electrons and holes (near the valence band region), increasing the mobility of the photoexcited carrier [51]. Along with the ground state band structure calculations, study of electron and hole masses, defect chemistry, photoexcited transport could be carried out to understand this system in detail. Understanding the excited state properties is useful in further development of new photocatalysts.

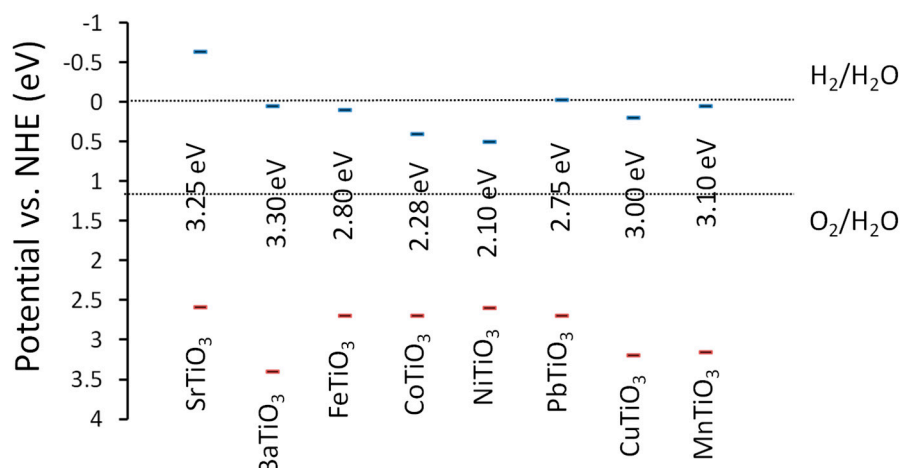
3.1.2. BaTiO₃

Like SrTiO₃, Rh doping in BaTiO₃ has been carried out and a quantum yield of 0.5% under 420 nm was reported [52]. Being a hydrogen evolving catalyst, this material has also been used as Z scheme with Pt/WO₃ for overall water splitting [52].

3.1.3. CaTiO₃

Calcium titanate is one of the common perovskite minerals with a band gap of 3.6 eV. Cu doping in CaTiO₃ is widely studied and visible light-driven photocatalytic water decomposition has been reported [53]. Cu doping not only induces visible light absorption, but also enhances hydrogen evolution under UV radiation when NiO_x co-catalyst is used. Studies of such doped systems, where dopants enhance the photocatalytic activity host materials are important to design efficient photocatalysts. Detrimental effects of doping on the properties such as electron-hole recombination, electron/hole effective mass, and reduced crystallinity should be studied and reported in detail. These studies are useful to gain insights on the photocatalytic activities of the doped systems. Co-doping of Ag and La at CaTiO₃ has been done to narrow the band gap and induce visible light absorption [54]. DFT studies also indicate that like SrTiO₃, TiO₂-terminated CaTiO₃ surfaces possess the capability of visible light absorption [55]. Along with alkali titanates, several transition metal titanates show promise for visible light photocatalysis. Figure 8 shows the empirically estimated band diagram of the MTiO₃ systems with respect to water oxidation and reduction levels.

Figure 8. Band edge potentials (vs. NHE; pH = 0) of MTiO₃ system [56].



Alkali metal titanates such as Ba, Ca, and Sr have enough CB potential for hydrogen evolution. However, certain transition metal titanates do not possess the desired CB potential for water reduction,

though they have band gap values in the visible region (such as Co, Ni, Fe *etc.*). These materials could be suitable for degradation of organics or other photooxidation reactions.

3.1.4. CoTiO₃

CoTiO₃ has a band gap in the visible region (E_g 2.28 eV). Recently this compound has been investigated for photocatalytic O₂ evolution reaction without any co-catalyst [57]. A yield of 64 $\mu\text{mol}\cdot\text{g}^{-1}\cdot\text{h}^{-1}$ was obtained under visible light. CoTiO₃ and TiO₂ composites have been studied for 2-propanol mineralization, however it is worth noting that the band positions of CoTiO₃ are not suitable for transferring photoexcited charges to TiO₂, offering no significant advantage [58].

3.1.5. NiTiO₃

NiTiO₃ has a reported band gap of around 2.16 eV and its light absorption spectra show peaks in visible region corresponding to crystal field splitting [59]. NiTiO₃ nanorods have been employed for degradation of nitrobenzene under visible light [59].

3.1.6. FeTiO₃

FeTiO₃ has a band gap of 2.8 eV and thus it absorbs visible light. Composites of FeTiO₃ and TiO₂ are studied for the degradation of 2-propenol under visible light. In such composites, TiO₂ acts as hole capturing phase, thereby separating the electron-hole recombination [60].

3.1.7. CdTiO₃

CdTiO₃ (E_g 2.8 eV) nanofibers were synthesized and studied for the photodegradation of rhodamine 6G (R6G) dye [61].

3.1.8. PbTiO₃

PbTiO₃ has a band gap of 2.75 eV and has been investigated for visible light photocatalysis. Core-shell particles of nano-TiO₂ (shell) and micro-PbTiO₃ (core) were studied for effective charge separation and photocatalytic performance [62]. It is worth noting that PbTiO₃ is ferroelectric in nature while TiO₂ is dielectric. It is shown that the ferroelectric behavior helps electron-hole separation at the interface of two particles.

3.1.9. MnTiO₃

Further, F doped MnTiO₃ shows improved separation of charges and degrades rhodamine B under visible light [63]. Some of the promising titanates photocatalysts have been listed in Table 1, as a part of compilation of perovskite systems.

Table 1. Compilation of promising photocatalytic systems for hydrogen or oxygen evolution under visible light.

Material System	Irradiation (nm)	Photocatalytic Performance	Experimental Details	Ref.
1% Rh doped SrTiO ₃ (0.5% Pt)	420–800	H ₂ at 48.1 μmol·h ⁻¹ with sacrificial agent	20% methanol, 50 mg in 50 mL of solution	[64]
Rh: SrTiO ₃ : BiVO ₄	>420	Z scheme Water splitting. H ₂ at 128, O ₂ at 61 μmol·h ⁻¹	4.2% Efficiency, 50 mg 120 mL (FeCl ₃ shuttle)	[46]
Cr-Sb co-doped SrTiO ₃ , (0.3% Pt)	>420	H ₂ at 78, O ₂ at 0.9 μmol·h ⁻¹ with sacrificial agents	in aqueous methanol and AgNO ₃ solution	[65]
MCo _{1/3} Nb _{2/3} O ₃ (0.2% Pt)	>420	H ₂ at 1.4 μmol·h ⁻¹ with sacrificial agent	500 mg catalyst in 50 mL methanol, 220 mL water,	[66]
Sr _{1-x} NbO ₃ (1% Pt)	>420	H ₂ at 44.8 μmol·h ⁻¹ with sacrificial agent	0.025M oxalic acid, 0.1g catalyst in 200 mL,	[67]
AgNbO ₃ -SrTiO ₃	>420	O ₂ at 162 μmol·h ⁻¹ with sacrificial agent	0.5 g catalyst in 275 mL AgNO ₃ solution,	[49]
LaFeO ₃ (Pt co-catalyst)	400–700	H ₂ at 3315 μmol·h ⁻¹ with sacrificial agent	H ₂ = 3315, μmol·h ⁻¹ , 1 mg in 20 mL of ethanol	[68]
CaTi _{1-x} Cu _x O ₃ (x = 0.02), NiO _x co-catalyst	>400	H ₂ at 22.7 μmol·h ⁻¹ with sacrificial agent	100 mg catalyst in 420 mL methanol solution	[53]
PrFeO ₃ , (Pt co-catalyst)	200W Tungsten source	H ₂ at 2847 μmol·h ⁻¹ with sacrificial agent	1 mg in 20 mL ethanol solution	[69]
Bi doped NaTaO ₃	>400	H ₂ at 59.48 μmol·h ⁻¹ with sacrificial agent	100 mg catalyst in 210 mL of methanol solution	[70]
GdCrO ₃ —Gd ₂ Ti ₂ O ₇ composite	>420	H ₂ at 246.3 μmol·h ⁻¹ with sacrificial agent	4.1% apparent quantum efficiency, methanol solution	[71]
CoTiO ₃	>420	O ₂ at 64.6 μmol·h ⁻¹ with sacrificial agent	100 mg in 100 mL 0.04M AgNO ₃ and La ₂ O ₃ solution, 420 nm	[57]

3.2. Tantalate Perovskites

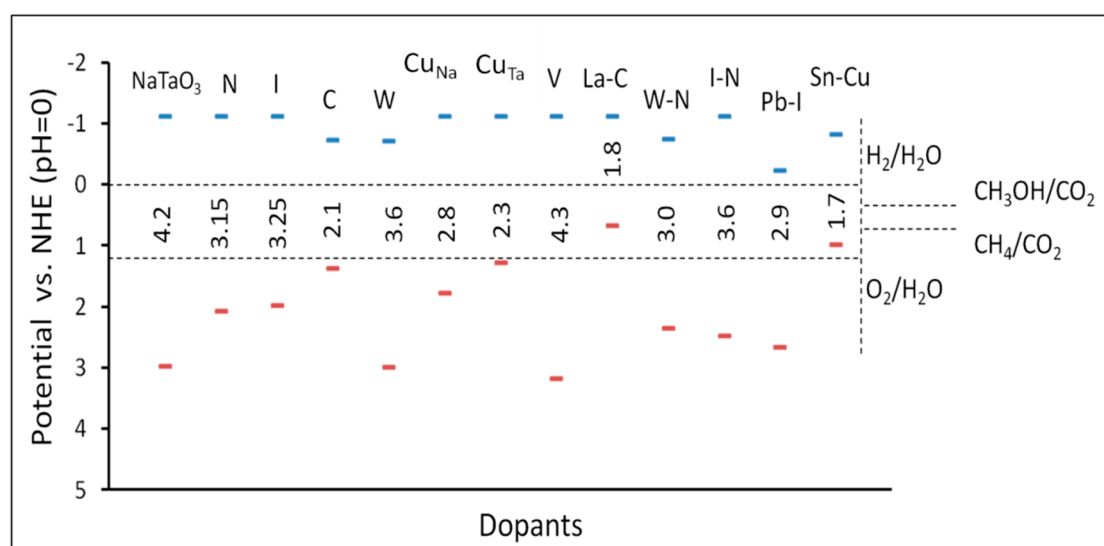
Alkali tantalates are particularly known for efficient overall water splitting reaction under UV irradiation as they possess both VB and CB potentials suitable for water splitting reaction [72–74]. To enable visible light photocatalysis, doping of various elements has been studied to achieve visible light activity.

3.2.1. NaTaO₃

Our group reported a detailed study on Bi-doped NaTaO₃ and showed that the bismuth doping site significantly affects the photocatalytic activity for hydrogen evolution [75,76]. Further, co-doping of La-Co, La-Cr, La-Ir, La-Fe in NaTaO₃ have shown successful visible light absorption and subsequent hydrogen evolution [77–81]. Co-doping of La-N in NaTaO₃ has been studied for hydrogen evolution by Zhao *et al.* [82]. These studies have indicated that both anion and cation doping in NaTaO₃ is useful for visible light photocatalytic applications. Among the doped NaTaO₃ systems, computational studies on the anionic (N, F, P, Cl, S) doping were reported by Han *et al.* which shows that certain anions like

N and P may be useful for visible light absorption [83]. Additionally, doping of magnetic cations such as Mn, Fe, and Co in NaTaO₃ has also been studied using DFT-PBE [84]. Recently, our group studied DFT calculations of a number of doped NaTaO₃-based photocatalysts by PBE0 hybrid calculations (Figure 9) [85]. Further, anion doping was also explored in detail using (HSE06) hybrid DFT calculations, where N, P, C, and S doping at O sites were studied. The study also reports the thermodynamics and effect of coupling between N-N, C-S, and P-P on the optical and electronic properties [86]. DFT studies are useful in explaining the properties of existing materials systems and designing new materials. Particularly, use of hybrid functional such as PBE0 or HSE06, is able to accurately define the valence band structure and location of bands or energy states that are crucially important for visible light driven photocatalysis. Hybrid DFT calculations could be useful in predictive modeling, where, band gaps and band edge potential of useful doped photocatalysts are identified. An example of doped tantalate systems is shown in Figure 9.

Figure 9. Estimated band gaps and band edge potentials of doped and co-doped NaTaO₃ systems: DFT study to design novel photocatalyst [85]



3.2.2. AgTaO₃

AgTaO₃ exhibits similar behavior to alkali tantalates, however, it has a smaller band gap value of 3.4 eV. AgTaO₃ doped with 30% Nb absorbs visible radiation and shows a stoichiometric overall water splitting reaction under visible light when loaded with NiO co-catalyst [87]. Co-doping of N-H and N-F in AgTaO₃ has been studied in detail. The study indicates that co-doping not only balances the charges but also improves the carrier mobility. N-F co-doped AgTaO₃ has an effective band gap value of 2.9 eV and shows H₂ generation under visible light [88].

3.2.3. KTaO₃

KTaO₃ (E_g 3.6 eV) photocatalysts have been studied for water splitting under UV radiation. However, work on development of visible light driven KTaO₃ based photocatalysts is limited.

3.3. Vanadium and Niobium Based Perovskites

Similar to tantalum (Ta)-based photocatalysts, Niobium (Nb)-based photocatalysts show good photocatalytic activity under UV irradiation.

3.3.1. KNbO₃ and NaNbO₃

Both KNbO₃ (E_g 3.14 eV) and NaNbO₃ (E_g 3.08 eV) have band gap values in the UV-responsive region, however suitable modifications of the band structure have resulted in visible light photocatalysis [89]. N-doped NaNbO₃ is a known visible light photocatalyst for the degradation of 2-propanol [90]. Nitrogen doping in KNbO₃ has been studied for water splitting as well as organic pollutant degradation [91]. First principles calculations predict that co-doping of La and Bi would induce visible light response in NaNbO₃ [92]. Recent work on ferroelectric perovskites of KNbO₃-BaNiNbO₃ shows that the solid solution of these compounds could absorb six times more light and shows fifty times more photocurrent than others [93]. Although photocatalytic properties are not known, this is an attractive candidate for visible light driven photocatalyst.

3.3.2. AgNbO₃

Replacing an A site alkali metal by silver reduces the band gap of the perovskite and AgNbO₃ has a band gap of around 2.7 eV. Studies have shown that the photocatalytic activity of AgNbO₃ strongly depends on the shape of the particles: polyhedron-shaped particles are favorable for O₂ evolution reactions [94]. Further, La doping was found to enhanced the hotocatalytic performance by 12-fold for gaseous 2-propenol degradation [95].

3.3.3. AgVO₃

AgVO₃ exists in two types of crystal structures, viz. α -AgVO₃ (E_g 2.5 eV) and β -AgVO₃ (E_g 2.3 eV) [96]. Both phases are photocatalytically active. However, β -AgVO₃ shows better photocatalytic performance than the α -phase. The CB potential of AgVO₃ is not sufficient for H₂ evolution, but it is suitable for the degradation of volatile organic compounds (VOCs) and O₂ evolution. β -AgVO₃ nanowires show excellent photocatalytic performance in the degradation of Rh B [97]. Composites of AgBr-AgVO₃ were reported to display respectable efficiency for Rh B degradation [98], while Ag-loaded AgVO₃ has shown good performance for degradation of bisphenol [99].

3.3.4. CuNbO₃

CuNbO₃ crystallizes in the monoclinic structure and has a band gap of 2.0 eV. It is an intrinsic p-type semiconductor and has shown 5% efficiency for photon to electron conversion when used as a photocathode. Being a stable material under irradiation, more investigations should be carried out on this material [100]. Tantalum, niobium, and vanadium belong to the same group in the periodic table. Perovskite compounds of these elements show decreasing band gap and CB potential values. This trend is attributed to the 3 d, 4 d and 5 d orbital energies in V, Nb and Ta, respectively.

3.4. Ferrite Perovskites

Most of the ferrite perovskites have their native band gaps in the visible region. Hematite and other iron oxide compounds have known shortcomings such as short exciton diffusion length, low electron conductivity, and lower conduction band edge potential [101]. However certain ferrite-based perovskites have shown good photocatalytic activities, circumventing the shortcomings seen in binary iron oxides.

3.4.1. LaFeO₃

LaFeO₃ (E_g 2.1 eV) has been explored for degradation of pollutants as well as hydrogen evolution under visible light. Sol-gel synthesized LaFeO₃ loaded with Pt co-catalyst showed high yield of hydrogen evolution ($3,315 \mu\text{mol}\cdot\text{h}^{-1}\cdot\text{g}^{-1}$, in the presence of ethanol) under 400 W tungsten light source [68]. Another study on this phase demonstrates high yield of H₂ and O₂ (1290 μmol and 640 μmol after three hours, respectively), without any co-catalyst loading [102]. Further, Thirumalairajan *et al.* showed shape dependent photocatalytic activity of LaFeO₃ for Rh B dye under visible light (>400 nm) [103]. Doping of Mn in LaFeO₃ has also been studied and it shows higher photocatalytic activity [104]. Lanthanum ferrite has demonstrated excellent photocatalytic activity under visible irradiation; however, studies on the fundamental photophysical properties are lacking the literature. Understanding the reasons why LaFeO₃ is a better photocatalyst than Fe₂O₃, in terms of comparative electronic properties such as electron-hole separation, mobility, photoexcited lifetimes *etc.* is important for further development in ferrite-based photocatalyst.

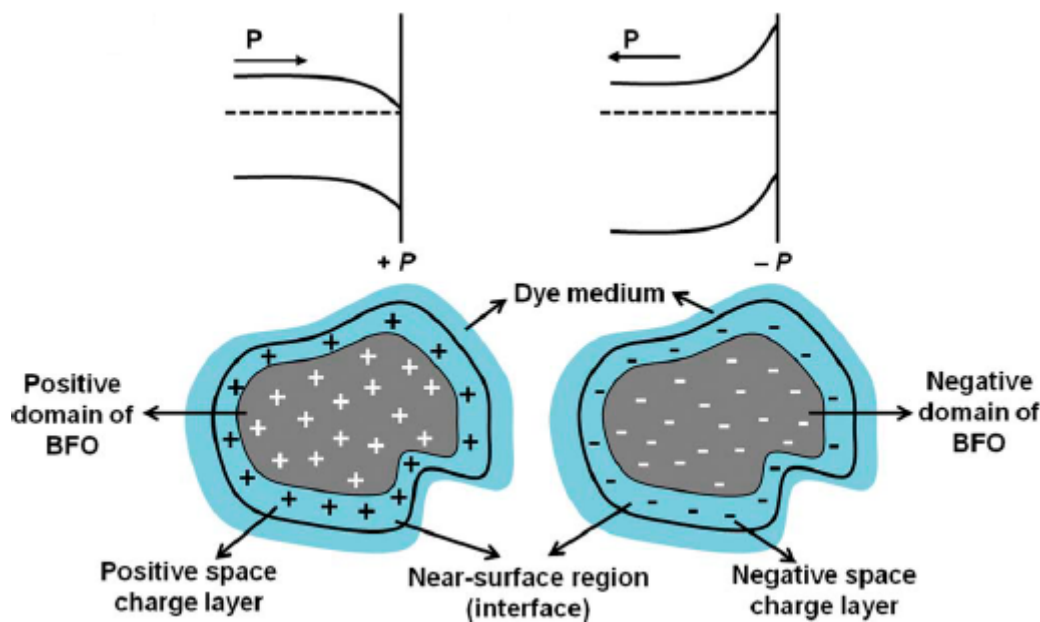
3.4.2. BiFeO₃

BiFeO₃ is a known ferroelectric material with a band gap of 2.3 eV. Recent studies have shown that BiFeO₃ could be used as a visible light photocatalyst [105]. The ferroelectric properties of BiFeO₃ could be utilized to enhance the electron-hole separation and improve the photocatalytic activity. Figure 10 shows the effect of polarization on the band bending of BiFeO₃ particles. Band bending affects the separation of electrons and holes in the space charge region and thus affects the photocatalytic activity. Gd-doped BiFeO₃ show enhanced photocatalytic degradation for rhodamine B degradation attributed to its ferromagnetic behavior [106]. Ca doping in BiFeO₃ leads to improved performance for photocatalytic degradation of Congo Red dye [107].

In another study, cations such as Y, Mg and Al were doped in BiFeO₃ and their photocatalytic performance was evaluated by degradation of Rh B under 400 nm radiation. The degradation performance was limited to C/C₀ of 0.8 within three hours [108]. The study of the effects of ferroelectric behavior on photocatalytic performance is a relatively new topic and it generally shows impressive activity for the degradation of organic pollutants, however, more experimental evidence and understanding are needed to establish a correlation between ferroelectric behavior and photocatalytic activity. Further studies on the stability and toxicity of bismuth-based materials should be carried out for realizing their practical applications. It is further noted that the tilting of octahedra in the perovskite crystal structure significantly affects its electronic properties. Nevertheless, the effect of tilting of octahedra on the photophysical properties such as electron-hole separation, electron transport,

delocalization of charges has not been studied in detail. Such studies will prove useful in establishing the importance of perovskites in the field of photocatalysis.

Figure 10. Schematics of changes to band diagram upon polarization of Gd doped BiFeO₃ due to ferroelectricity [106].



3.4.3. GaFeO₃

GaFeO₃ has been reported to show overall water splitting without any co-catalyst loading under visible light ($\lambda > 395$ nm) [109]. The authors also reported a yield of 0.10 and 0.04 $\mu\text{mol}\cdot\text{h}^{-1}$ under a 450 nm band pass filter. It is worth noting that the catalytic activity decreased due to deactivation of the catalyst.

3.4.4. YFeO₃

Among the other ferrites, YFeO₃ has a band gap value of 2.43 eV and showed photocatalytic activity four times that of TiO₂-P25 under > 400 nm visible light radiation (Rh B degradation) [110].

3.4.5. PrFeO₃

PrFeO₃ was evaluated for hydrogen evolution reaction from ethanol-water mixture and showed a yield of 2847 $\mu\text{mol}\cdot\text{g}^{-1}\cdot\text{h}^{-1}$ under 200W tungsten lamp irradiation [69].

3.4.6. AlFeO₃

Composites of AlFeO₃ and TiO₂ are reported to yield the sunlight driven photocatalytic degradation of methyl orange (MO) and eosin dye [111]. Ferrite based perovskites also offer advantage of magnetic recovery of the particles which is useful in practical applications.

3.5. Other Perovskite Systems

Among the other perovskite photocatalysts, compounds of bismuth, cobalt, nickel, and antimony (occupying B sites) have band gap values in the visible region. Pentavalent bismuth perovskites are known to be active photocatalysts under visible light radiation. Perovskites such as LiBiO_3 (E_g 1.63 eV), NaBiO_3 (E_g 2.53 eV), KBiO_3 (E_g 2.04 eV), and AgBiO_3 (E_g 2.5 eV) have all been investigated for degradation of organic pollutants [112]. NaBiO_3 shows better photocatalytic performance for phenol and methylene blue (MB) degradation as compared to other Bi^{5+} containing perovskites as well as P25-TiO₂ [112]. NaBiO_3 is also reported to have higher photocatalytic activity than N-doped TiO₂ photocatalyst [113]. NaBiO_3 and BiOCl composites have been studied for enhanced electron-hole separation and subsequent photocatalysis [114]. AgBiO_3 was shown to be effective in restricting the growth of *Microcystis aeruginosa* under simulated solar light [115]. This study shows that AgBiO_3 with band gap energy around 2.5 eV could be a potential algaecide under natural light. DFT studies show that NaBiO_3 has a strong band dispersion arising from Na 3s and O 2p hybridized orbitals, which contributes to the higher photocatalytic activity [112]. LaCoO_3 has a band gap value of 2.7 eV and oxygen deficient $\text{LaCoO}_{3-\delta}$ ($\text{LaCoO}_{3-\delta}$) has been studied for MO degradation (>400 nm) [116].

Other compounds such as LaNiO_3 has been studied for MO degradation using wavelengths greater than 400 nm [117]. Cu doping in LaNiO_3 has been studied for improved H₂ evolution [118]. Ilmenite type AgSbO_3 has an absorption edge onset at 480 nm, and it has been demonstrated for O₂ evolution under sacrificial agent as well as degradation of MB, RhB, and 4-chlorophenol [119]. Further, solid solution of LaCrO_3 and $\text{Na}_{0.5}\text{La}_{0.5}\text{TiO}_3$ was developed for hydrogen evolution [120]. Recently, $\text{Gd}_2\text{Ti}_2\text{O}_7/\text{GdCrO}_3$ composite was reported as photocatalyst p-n junction photocatalyst [71]. The study shows that GdCrO_3 has a band gap of 2.5 eV and is responsible for the visible light absorption [72].

4. Complex Perovskite Materials

4.1. Double Perovskites

Compounds with general formula $\text{A}_2\text{B}_2\text{O}_6$ belong to the double perovskites and they have similar crystal structures to simple perovskites. Double perovskites have the basic framework of corner connected BO₆ octahedra and A cations enclosed within, however, the connectivity of the octahedra may differ from structure to structure. Double perovskites could accommodate different cations at the A or/and B sites, taking a general form AA'BB'O₆. Accommodation of different cations at the A and B sites alters the photophysical properties of the compound significantly. Among the binary oxides, only a few compounds are known to have band gap values in the visible region (narrow gap), e.g., Fe_2O_3 , WO_6 , CuO , Bi_2O_3 . However, these materials suffer from insufficient CB potential for hydrogen evolution. Some of the materials also suffer from poor stability and low mobility of photoexcited charges. On the other hand, many of the binary oxides are known to be efficient photocatalysts, however only activated by UV radiation (wide gap). Complex compounds offer a possibility of combining the elements from ‘narrow gap’ and ‘wide gap’ binary compounds to exploit the properties of both types of oxides, and thus are potentially useful as visible light photocatalysts. The following section reviews photocatalytic properties of double perovskites which are visible light active.

4.1.1. Sr₂FeNbO₆

Sr₂FeNbO₆ has a cubic crystal structure and a band gap of 2.06 eV. In its pristine form, it is a known photocatalyst, while 7% Ti doping at Fe site has shown two time enhancement of the hydrogen generation in methanol solution. A total of 28.5 $\mu\text{mol}\cdot\text{h}^{-1}$ and 650 $\mu\text{mol}\cdot\text{h}^{-1}$ were reported in presence of sacrificial agents and with 0.2% Pt as co-catalyst [121]. W doping in Sr₂FeNbO₆ has also been studied and demonstrated enhancement to hydrogen evolution under visible radiation [122].

4.1.2. La₂FeTiO₆

Hu *et al.* reported higher photocatalytic activity for La₂FeTiO₆ than for LaFeO₃ for degradation of *p*-chlorophenol under visible light irradiation [123].

4.1.3. Other Double Perovskites

Rare earth and bismuth-based double perovskites were studied for visible light photocatalysis. Compounds with general formula Ba₂RBiO₆, (R = La, Ce, Pr, Nd, Sm, Eu, Gd, Dy), were prepared and their photocatalytic activity was studied for MB degradation [124]. Authors found rare earth cation dependent photocatalytic performance, where compounds such as Ba₂EuBiO₆, Ba₂SmBiO₆, and Ba₂CeBiO₆ showed high photocatalytic activity. Complex perovskites such as CaCu₃Ti₄O₁₂ have also been studied for their photocatalytic performance. CaCu₃Ti₄O₁₂ was found to possess an indirect band gap of 1.27 eV and Pt-loaded CaCu₃Ti₄O₁₂ shows degradation of MO under radiation greater than 420 nm [125]. Photophysical properties of certain double perovskite compounds have been reported, however, more efforts are needed to investigate photocatalytic properties of these materials. Compounds such as Ba₂CoWO₆, Ba₂NiWO₆, Sr₂CoWO₆ and Sr₂NiWO₆ are stable perovskites compounds for O₂ evolution using sacrificial agents [126].

Certain tantalum-based compounds have been studied for degradation of organic compounds. N-doped K₂Ta₂O₆ is known to absorb visible light up to 600 nm and degrade formaldehyde under visible light [127]. Our group demonstrated that Bi doping in Na₂Ta₂O₆ causes visible light absorption and degradation of MB [128]. Although some work has been done with double perovskites as photocatalysts, understanding of their fundamental properties is limited. More work is needed to discover their advantages as visible light photocatalyst and develop novel materials systems.

4.2. Mixed Oxides

Mixture of oxides and nitrides or oxides and sulphides has been developed to engineer the band structure of the oxide photocatalysts suitable for the visible light absorption. Oxynitride and oxysulphide photocatalysts offer distinctive advantages over their doped counterparts. Earlier reports on oxynitrides have revealed that replacing oxygen by nitrogen at lattice sites, in a stoichiometric manner, narrows the band gap of the oxide, by pushing the VBM into the band gap [129]. Such a modification does not produce native point defects, which would otherwise be introduced in the case of N doping. Stoichiometric incorporation of nitrogen also avoids the localized states induced by N doping and reduces the possible electron-hole recombination. Similar composition containing mixtures of sulfur and oxygen *i.e.*, oxysulfides, has been developed for photocatalysts. Mixed oxysulfide

perovskites of $\text{Sm}_2\text{Ti}_2\text{S}_2\text{O}_5$ (E_g 2.0 eV) is known for water oxidation and reduction reaction for oxygen and hydrogen evolution, respectively in presence of sacrificial agents under low photon energy wavelengths of 650 nm. The band structure of this phase reveals that the presence of sulphur narrows the band gap and enables visible light absorption [130].

Oxynitride compounds such as CaNbO_2N , SrNbO_2N , BaNbO_2N , and LaNbON_2 belong to the perovskite type crystal structures [131]. Photocatalytic hydrogen evolution has been reported under visible light from methanol solution. SrNbO_2N (E_g 1.8 eV) has been investigated in detail, where the photoelectrode of SrNbO_2N on a transparent conducting surface shows water oxidation reaction under no external bias [132]. Tantalum counterparts of these compounds were developed and utilized in the Z scheme photocatalysis. Compounds such as CaTaO_2N and BaTaO_2N were loaded with Pt co-catalyst and coupled with pt/ WO_3 for Z scheme water splitting [133]. A solid solution of BaTaO_2N and BaZrO_3 was formulated for hydrogen and oxygen evolution, which showed improved performance compared with the individual photocatalysts under visible light [134]. LaTiO_xN_y is another perovskite type compound which shows high photocurrent density under visible light [135].

Apart from the double perovskites belonging to the general formula $\text{AA}'\text{BB}'\text{O}_6$, there are several other compounds that show crystal structures close to the perovskite type structure, however such compounds are not included in the current review. Theoretically, double perovskites offer a wider scope to design photocatalysts by selecting suitable cations and AA' and BB' sites in the lattice. Work on design and development of double perovskite is currently limited and synthesis and characterization of new materials in this category are needed.

5. Summary and Outlook

A large number of perovskite-based compounds (over 80) have been studied for visible light driven photocatalytic applications. Perovskite structures offer abundant scope in designing novel compounds based on A and B site occupancy, which gives rise to a wide range of materials systems with unique properties. Among these compounds, photocatalysts with pristine band gaps in the visible region such as LaFeO_3 , PrFeO_3 , NaBiO_3 , and AgBiO_3 (Table 2) show promising photocatalytic performance under visible radiation (>400 nm). Although there are reports on the photocatalytic activity of these compounds, detailed studies on these materials are limited. More efforts are needed to understand the structure-property relations in such ferrites and bismuth based compounds and improve their photocatalytic activity. Among the wide band gap semiconductors, SrTiO_3 - and NaTaO_3 -based photocatalysts are the most investigated systems. The strategy of doping foreign elements in wide band gap photocatalysts is widely used to induce visible light absorption and subsequently to enable photocatalytic activity. Nonetheless, very limited knowledge is available on the adverse effect of dopants on the photophysical properties of the compounds (e.g., if the benefit derived from dopant-induced visible light activity is outweighed by a loss of UV light activity). This should be properly investigated in the future. Appropriate dopants which retain the beneficial properties of the host materials while inducing visible light responses should be identified. Research work on complex perovskites show that these compounds offer distinct advantages as compared with simple perovskites. Designing complex perovskite compounds with suitable elements at A and B sites to yield desired photocatalytic properties is a challenge. We expect computational design would help shorten the

selection process. Recent advances in computational tools such as DFT based band structure calculations are highly effective to design and understand novel materials systems.

Table 2. Compilation of promising photocatalytic systems for organic compounds degradation under visible light.

Materials System	Band Gap (eV)	Photocatalytic Tests Reported	Ref.
Ga doped BiFeO ₃	2.18–2.50	Enhanced degradation of rhodamine B compared to pristine BiFeO ₃	[106]
LaFeO ₃	2.10	Nanospheres show higher rates of rhodamine B degradation than nanocubes and nanorods	[103]
YFeO ₃	2.43	Rhodamine B degradation rate higher than P25 (>400 nm)	[110]
NaBiO ₃	2.60	Bleaching rate of Methylene Blue higher than N doped TiO ₂ . (>400 nm)	[113]
AgSbO ₃	2.58	Efficient degradation of Rh B. MB, 4-chlorophenol (>420 nm)	[119,136]
AgBiO ₃	2.50	Inhibition of <i>Microcystis</i>	[115]

As certain perovskite compounds exhibit ferroelectric, ferromagnetic, or piezoelectric effects, there is a need to understand the correlation between these effects and the photocatalytic activity to a greater depth. Such studies would certainly be helpful in the development of efficient visible light photocatalysts. On a final note, there has been significant progress in the development of visible light perovskites in the past years. This development has laid a good foundation for future work in this area. Further understanding of the crystal and electronic structural factors behind photocatalytic activity is needed for the future development of efficient visible light-driven perovskites.

Acknowledgments

Financial support through an SUG grant from the College of Engineering, Nanyang Technological University, Singapore is greatly appreciated.

Author Contributions

P.K. performed literature research, analysis, and drafted the paper. C.Z. initiated and supervised the work and provided insights. Both authors revised and approved the final manuscript.

Conflicts of Interest

The authors declare no conflict of interest.

References

1. Maeda, K. Photocatalytic water splitting using semiconductor particles: History and recent developments. *J. Photochem. Photobiol. C* **2011**, *12*, 237–268.
2. Qu, Y. Duan, X. Progress, challenge and perspective of heterogeneous photocatalysts. *Chem. Soc. Rev.* **2013**, *42*, 2568–2580.
3. Hou, W.; Cronin, S.B. A Review of Surface Plasmon Resonance-Enhanced Photocatalysis. *Adv. Funct. Mat.* **2013**, *23*, 1612–1619.

4. Osterloh, F.E. Inorganic nanostructures for photoelectrochemical and photocatalytic water splitting. *Chem. Soc. Rev.* **2013**, *42*, 2294–2320.
5. Cook, T.R.; Dogutan, D.K.; Reece, S.Y.; Surendranath, Y.; Teets, T.S.; Nocera, D.G. Solar energy supply and storage for the legacy and nonlegacy worlds. *Chem. Rev.* **2010**, *110*, 6474–6502.
6. Izumi, Y. Recent advances in the photocatalytic conversion of carbon dioxide to fuels with water and/or hydrogen using solar energy and beyond. *Coord. Chem. Rev.* **2013**, *257*, 171–186.
7. Tahir, M.; Amin, N.S. Recycling of carbon dioxide to renewable fuels by photocatalysis: Prospects and challenges. *Renew. Sust. Energy Rev.* **2013**, *25*, 560–579.
8. Tan, Y.N.; Wong, C.L.; Mohamed, A.R. An Overview on the Photocatalytic Activity of Nano-Doped-TiO₂ in the Degradation of Organic Pollutants. *ISRN Mat. Sci.* **2011**, *2011*, 18.
9. Pelaez, M.; Nolan, N.T.; Pillai, S.C.; Seery, M.K.; Falaras, P.; Kontos, A.G.; Dunlop, P.S.M.; Hamilton, J.W.J.; Byrne, J.A.; O’shea, K.; *et al.* A review on the visible light active titanium dioxide photocatalysts for environmental applications. *Appl. Catal. B* **2012**, *125*, 331–349.
10. Dalrymple, O.K.; Stefanakos, E.; Trotz, M.A. Goswami, D.Y. A review of the mechanisms and modeling of photocatalytic disinfection. *Appl. Catal. B* **2010**, *98*, 27–38.
11. Zhang, Z.; Gamage, J. Applications of photocatalytic disinfection. *Int. J. Photoenergy* **2010**, doi:10.1155/2010/764870.
12. Konstantinou, I.K.; Albanis, T.A. TiO₂-assisted photocatalytic degradation of azo dyes in aqueous solution: Kinetic and mechanistic investigations: A review. *Appl. Catal. B* **2004**, *49*, 1–14.
13. Ahmed, S.; Rasul, M.G.; Martens, W.; Brown, R.; Hashib, M.A. Advances in Heterogeneous Photocatalytic Degradation of Phenols and Dyes in Wastewater: A Review. *Water Air Soil Pollut.* **2011**, *215*, 3–29.
14. Rajesh, J.T.; Praveen, K.S.; Ramchandra, G.K.; Raksh, V.J. Photocatalytic degradation of dyes and organic contaminants in water using nanocrystalline anatase and rutile TiO₂. *Sci. Technol. Adv. Mat.* **2007**, *8*, 455.
15. Bickley, R.I.; Vishwanathan, V. Photocatalytically induced fixation of molecular nitrogen by near UV radiation. *Nature* **1979**, *280*, 306–308.
16. Guo, C.; Wu, X.; Yan, M.; Dong, Q.; Yin, S.; Sato, T.; Liu, S. The visible-light driven photocatalytic destruction of NO_x using mesoporous TiO₂ spheres synthesized via a “water-controlled release process”. *Nanoscale* **2013**, *5*, 8184–8191.
17. Zhao, J.; Yang, X. Photocatalytic oxidation for indoor air purification: A literature review. *Build. Environ.* **2003**, *38*, 645–654.
18. Lasek, J.; Yu, Y.-H.; Wu, J.C.S. Removal of NO_x by photocatalytic processes. *J. Photchem. Photobiol. C* **2013**, *14*, 29–52.
19. Wang, H.; Wu, Z.; Zhao, W.; Guan, B. Photocatalytic oxidation of nitrogen oxides using TiO₂ loading on woven glass fabric. *Chemosphere* **2007**, *66*, 185–190.
20. Bhalla, A.S.; Guo, R.; Roy, R. The perovskite structure—a review of its role in ceramic science and technology. *Mat. Res. Innov.* **2000**, *4*, 3–26.
21. Damjanovic, D. Piezoelectric properties of perovskite ferroelectrics: unsolved problems and future research. *Ann. Chim.-Sci. Mat.* **2001**, *26*, 99–106.
22. Nuraje, N.; Su, K. Perovskite ferroelectric nanomaterials. *Nanoscale* **2013**, *5*, 8752–8780.

23. Jia, Q.; Iwase, A.; Kudo, A. BiVO₄-Ru/SrTiO₃:Rh composite Z-scheme photocatalyst for solar water splitting. *Chem. Sci.* **2014**, *5*, 1513–1519.
24. Sayama, K.; Mukasa, K.; Abe, R.; Abe, Y.; Arakawa, H. Stoichiometric water splitting into H₂ and O₂ using a mixture of two different photocatalysts and an IO₃[−]/I[−] shuttle redox mediator under visible light irradiation. *Chem. Commun.* **2001**, *23*, 2416–2417.
25. Zhang, W.F.; Tang, J.; Ye, J. Photoluminescence and photocatalytic properties of SrSnO₃ perovskite. *Chem. Phys. Lett.* **2006**, *418*, 174–178.
26. Lin, W.H.; Cheng, C.; Hu, C.C.; Teng, H. NaTaO₃ photocatalysts of different crystalline structures for water splitting into H₂ and O₂. *Appl. Phys. Lett.* **2006**, *89*, 211904.
27. Shi, J.; Guo, L. ABO₃-based photocatalysts for water splitting. *Prog. Nat. Sci. Mat. Int.* **2012**, *22*, 592–615.
28. Wang, W.N.; Soulis, J.; Jeffrey Yang, Y.; Biswas, P. Comparison of CO₂ photoreduction systems: A review. *Aerosol Air Qual. Res.* **2014**, *14*, 533–549.
29. Tang, J.; Durrant, J.R.; Klug, D.R. Mechanism of Photocatalytic Water Splitting in TiO₂. Reaction of Water with Photoholes, Importance of Charge Carrier Dynamics, and Evidence for Four-Hole Chemistry. *J. Am. Chem. Soc.* **2008**, *130*, 13885–13891.
30. Kudo, A.; Miseki, Y. Heterogeneous photocatalyst materials for water splitting. *Chem. Soc. Rev.* **2009**, *38*, 253–278.
31. Houas, A.; Lachheb, H.; Ksibi, M.; Elaloui, E.; Guillard, C.; Herrmann, J.-M. Photocatalytic degradation pathway of methylene blue in water. *Appl. Catal. B* **2001**, *31*, 145–157.
32. Cho, M.; Chung, H.; Choi, W.; Yoon, J. Linear correlation between inactivation of *E. coli* and OH radical concentration in TiO₂ photocatalytic disinfection. *Water Res.* **2004**, *38*, 1069–1077.
33. Turchi, C.S.; Ollis, D.F. Photocatalytic degradation of organic water contaminants: Mechanisms involving hydroxyl radical attack. *J. Catal.* **1990**, *122*, 178–192.
34. Haberreutinger, S.N.; Schmidt-Mende, L.; Stolarsky, J.K. Photocatalytic reduction of CO₂ on TiO₂ and other semiconductors. *Angew. Chem. Int. Ed.* **2013**, *52*, 7372–7408.
35. Rusina, O.; Linnik, O.; Eremenko, A.; Kisch, H. Nitrogen Photofixation on Nanostructured Iron Titanate Films. *Chem. Eur. J.* **2003**, *9*, 561–565.
36. Rusina, O.; Macyk, W.; Kisch, H. Photoelectrochemical Properties of a Dinitrogen-Fixing Iron Titanate Thin Film. *J. Phys. Chem. B* **2005**, *109*, 10858–10862.
37. Zhu, D.; Zhang, L.; Ruther, R.E.; Hamers, R.J. Photo-illuminated diamond as a solid-state source of solvated electrons in water for nitrogen reduction. *Nat. Mater.* **2013**, *12*, 836–841.
38. Kavan, L.; Grätzel, M.; Gilbert, S.; Klemenz, C.; Scheel, H. Electrochemical and photoelectrochemical investigation of single-crystal anatase. *J. Am. Chem. Soc.* **1996**, *118*, 6716–6723.
39. Van Benthem, K.; Elsässer, C.; French, R.H. Bulk electronic structure of SrTiO₃: Experiment and theory. *J. Appl. Phys.* **2001**, *90*, 6156–6164.
40. Townsend, T.K.; Browning, N.D.; Osterloh, F.E. Overall photocatalytic water splitting with NiOx-SrTiO₃—A revised mechanism. *Energy Environ. Sci.* **2012**, *5*, 9543–9550.
41. Konta, R.; Ishii, T.; Kato, H.; Kudo, A. Photocatalytic Activities of Noble Metal Ion Doped SrTiO₃ under Visible Light Irradiation. *J. Phys. Chem. B* **2004**, *108*, 8992–8995.

42. Chen, H.-C.; Huang, C.-W.; Wu, J.C.S.; Lin, S.-T. Theoretical Investigation of the Metal-Doped SrTiO₃ Photocatalysts for Water Splitting. *J. Phys. Chem. C* **2012**, *116*, 7897–7903.
43. Iwashina, K.; Kudo, A. Rh-Doped SrTiO₃ Photocatalyst Electrode Showing Cathodic Photocurrent for Water Splitting under Visible-Light Irradiation. *J. Am. Chem. Soc.* **2011**, *133*, 13272–13275.
44. Sasaki, Y.; Kato, H.; Kudo, A. [Co(bpy)₃]^{3+/2+} and [Co(phen)₃]^{3+/2+} Electron Mediators for Overall Water Splitting under Sunlight Irradiation Using Z-Scheme Photocatalyst System. *J. Am. Chem. Soc.* **2013**, *135*, 5441–5449.
45. Sasaki, Y.; Nemoto, H.; Saito, K.; Kudo, A. Solar Water Splitting Using Powdered Photocatalysts Driven by Z-Schematic Interparticle Electron Transfer without an Electron Mediator. *J. Phys. Chem. C* **2009**, *113*, 17536–17542.
46. Kato, H.; Sasaki, Y.; Shirakura, N.; Kudo, A. Synthesis of highly active rhodium-doped SrTiO₃ powders in Z-scheme systems for visible-light-driven photocatalytic overall water splitting. *J. Mater. Chem. A* **2013**, *1*, 12327–12333.
47. Asai, R.; Nemoto, H.; Jia, Q.; Saito, K.; Iwase, A.; Kudo, A. A visible light responsive rhodium and antimony-codoped SrTiO₃ powdered photocatalyst loaded with an IrO₂ cocatalyst for solar water splitting. *Chem. Commun.* **2014**, *50*, 2543–2546.
48. Jia, Y.; Shen, S.; Wang, D.; Wang, X.; Shi, J.; Zhang, F.; Han, H.; Li, C. Composite Sr₂TiO₄/SrTiO₃(La,Cr) heterojunction based photocatalyst for hydrogen production under visible light irradiation. *J. Mater. Chem. A* **2013**, *1*, 7905–7912.
49. Wang, D.; Kako, T.; Ye, J. New Series of Solid-Solution Semiconductors (AgNbO₃)_{1-x}(SrTiO₃)_x with Modulated Band Structure and Enhanced Visible-Light Photocatalytic Activity. *J. Phys. Chem. C* **2009**, *113*, 3785–3792.
50. Fu, Q.; He, T.; Li, J.L.; Yang, G.W. Band-engineered SrTiO₃ nanowires for visible light photocatalysis. *J. Appl. Phys.* **2012**, *112*, 104322.
51. Wunderlich, W.; Ohta, H.; Koumoto, K. Enhanced effective mass in doped SrTiO₃ and related perovskites. *Physica B* **2009**, *404*, 2202–2212.
52. Maeda, K. Rhodium-Doped Barium Titanate Perovskite as a Stable p-Type Semiconductor Photocatalyst for Hydrogen Evolution under Visible Light. *ACS App. Mater. Interfaces* **2014**, *6*, 2167–2173.
53. Zhang, H.; Chen, G.; Li, Y.; Teng, Y. Electronic structure and photocatalytic properties of copper-doped CaTiO₃. *Int. J. Hydrg. Energy* **2010**, *35*, 2713–2716.
54. Zhang, H.; Chen, G.; He, X.; Xu, J. Electronic structure and photocatalytic properties of Ag–La codoped CaTiO₃. *J. Alloys Compd.* **2012**, *516*, 91–95.
55. Fu, Q.; Li, J.L.; He, T.; Yang, G.W. Band-engineered CaTiO₃ nanowires for visible light photocatalysis. *J. Appl. Phys.* **2013**, *113*, 104303.
56. Xu, Y.; Schoonen, M.A. The absolute energy positions of conduction and valence bands of selected semiconducting minerals. *Am. Miner.* **2000**, *85*, 543–556.
57. Qu, Y.; Zhou, W.; Fu, H. Porous Cobalt Titanate Nanorod: A New Candidate for Visible Light-Driven Photocatalytic Water Oxidation. *ChemCatChem* **2014**, *6*, 265–270.
58. Rawal, S.B.; Bera, S.; Lee, D.; Jang, D.-J.; Lee, W.I. Design of visible-light photocatalysts by coupling of narrow bandgap semiconductors and TiO₂: Effect of their relative energy band positions on the photocatalytic efficiency. *Catal. Sci. Technol.* **2013**, *3*, 1822–1830.

59. Qu, Y.; Zhou, W.; Ren, Z.; Du, S.; Meng, X.; Tian, G.; Pan, K.; Wang, G.; Fu, H. Facile preparation of porous NiTiO₃ nanorods with enhanced visible-light-driven photocatalytic performance. *J. Mater. Chem.* **2012**, *22*, 16471–16476.
60. Kim, Y.J.; Gao, B.; Han, S.Y.; Jung, M.H.; Chakraborty, A.K.; Ko, T.; Lee, C.; Lee, W.I. Heterojunction of FeTiO₃ Nanodisc and TiO₂ Nanoparticle for a Novel Visible Light Photocatalyst. *J. Phys. Chem. C* **2009**, *113*, 19179–19184.
61. Hassan, M.A.; Amna, T.; Khil, M.-S. Synthesis of High aspect ratio CdTiO₃ nanofibers via electrospinning: characterization and photocatalytic activity. *Ceram. Int.* **2014**, *40*, 423–427.
62. Li, L.; Zhang, Y.; Schultz, A.M.; Liu, X.; Salvador, P.A.; Rohrer, G.S. Visible light photochemical activity of heterostructured PbTiO₃-TiO₂ core-shell particles. *Catal. Sci. Technol.* **2012**, *2*, 1945–1952.
63. Dong, W.; Wang, D.; Jiang, L.; Zhu, H.; Huang, H.; Li, J.; Zhao, H.; Li, C.; Chen, B.; Deng, G. Synthesis of F doping MnTiO₃ nanodiscs and their photocatalytic property under visible light. *Mater. Lett.* **2013**, *98*, 265–268.
64. Shen, P.; Lofaro, J.C., Jr.; Woerner, W.R.; White, M.G.; Su, D.; Orlov, A. Photocatalytic activity of hydrogen evolution over Rh doped SrTiO₃ prepared by polymerizable complex method. *Chem. Eng. J.* **2013**, *223*, 200–208.
65. Kato, H.; Kudo, A. Visible-Light-Response and Photocatalytic Activities of TiO₂ and SrTiO₃ Photocatalysts Codoped with Antimony and Chromium. *J. Phys. Chem. B* **2002**, *106*, 5029–5034.
66. Yin, J.; Zou, Z.; Ye, J. A Novel Series of the New Visible-Light-Driven Photocatalysts MCo_{1/3}Nb_{2/3}O₃ (M = Ca, Sr, and Ba) with Special Electronic Structures. *J. Phys. Chem. B* **2003**, *107*, 4936–4941.
67. Xu, X.; Randorn, C.; Efstrathiou, P.; Irvine, J.T.S. A red metallic oxide photocatalyst. *Nat. Mater.* **2012**, *11*, 595–598.
68. Tijare, S.N.; Joshi, M.V.; Padole, P.S.; Mangrulkar, P.A.; Rayalu, S.S.; Labhsetwar, N.K. Photocatalytic hydrogen generation through water splitting on nano-crystalline LaFeO₃ perovskite. *Int. J. Hydron. Energy* **2012**, *37*, 10451–10456.
69. Tijare, S.N.; Bakardjieva, S.; Subrt, J.; Joshi, M.V.; Rayalu, S.S.; Hishita, S.; Labhsetwar, N. Synthesis and visible light photocatalytic activity of nanocrystalline PrFeO₃ perovskite for hydrogen generation in ethanol–water system. *J. Chem. Sci.* **2014**, *126*, 517–525.
70. Li, Z.; Wang, Y.; Liu, J.; Chen, G.; Li, Y.; Zhou, C. Photocatalytic hydrogen production from aqueous methanol solutions under visible light over Na(Bi_xTa_{1-x})O₃ solid-solution. *Int. J. Hydron. Energy* **2009**, *34*, 147–152.
71. Parida, K.M.; Nashim, A.; Mahanta, S.K. Visible-light driven Gd₂Ti₂O₇/GdCrO₃ composite for hydrogen evolution. *J. Chem. Soc. Dalton Trans.* **2011**, *40*, 12839–12845.
72. Kato, H.; Asakura, K.; Kudo, A. Highly efficient water splitting into H₂ and O₂ over lanthanum-doped NaTaO₃ photocatalysts with high crystallinity and surface nanostructure. *J. Am. Chem. Soc.* **2003**, *125*, 3082–3089.
73. Yamakata, A.I.T.A.; Kato, H.; Kudo, A.; Onishi, H. Photodynamics of NaTaO₃ Catalysts for Efficient Water Splitting. *J. Phys. Chem. B* **2003**, *107*, 14383–14387.
74. Kato, H.; Kudo, A. Water splitting into H₂ and O₂ on alkali tantalate photocatalysts ATaO₃ (A = Li, Na, and K). *J. Phys. Chem. B* **2001**, *105*, 4285–4292.

75. Kanhere, P.D.; Zheng, J.; Chen, Z. Site Specific Optical and Photocatalytic Properties of Bi-Doped NaTaO₃. *J. Phys. Chem. C* **2011**, *115*, 11846–11853.
76. Kanhere, P.; Zheng, J.; Chen, Z. Visible light driven photocatalytic hydrogen evolution and photophysical properties of Bi³⁺ doped NaTaO₃. *Int. J. Hydrg. Energy* **2012**, *37*, 4889–4896.
77. Yi, Z.G.; Ye, J.H. Band gap tuning of Na_{1-x}La_xTa_{1-x}Co_xO₃ solid solutions for visible light photocatalysis. *App. Phys. Lett.* **2007**, *91*, 254108.
78. Yi, Z.G.; Ye, J.H. Band gap tuning of Na_{1-x}La_xTa_{1-x}Cr_xO₃ for H₂ generation from water under visible light irradiation. *J. App. Phys.* **2009**, *106*, 074910.
79. Yang, M.; Huang, X.; Yan, S.; Li, Z.; Yu, T.; Zou, Z. Improved hydrogen evolution activities under visible light irradiation over NaTaO₃ codoped with lanthanum and chromium. *Mater. Chem. Phys.* **2010**, *121*, 506–510.
80. Iwase, A.; Saito, K.; Kudo, A. Sensitization of NaMO₃ (M: Nb and Ta) photocatalysts with wide band gaps to visible light by Ir doping. *Bull. Chem. Soc. Jpn.* **2009**, *82*, 514–518.
81. Kanhere, P.; Nisar, J.; Tang, Y.; Pathak, B.; Ahuja, R.; Zheng, J.; Chen, Z. Electronic Structure, Optical Properties, and Photocatalytic Activities of LaFeO₃–NaTaO₃ Solid Solution. *J. Phys. Chem. C* **2012**, *116*, 22767–22773.
82. Zhao, Z.; Li, R.; Li, Z.; Zou, Z. Photocatalytic activity of La-N-codoped NaTaO₃ for H₂ evolution from water under visible-light irradiation. *J. Phys. D Appl. Phys.* **2011**, *44*, 165401.
83. Han, P.; Wang, X.; Zhao, Y.H.; Tang, C. Electronic structure and optical properties of non-metals (N, F, P, Cl, S)—Doped cubic NaTaO₃ by density functional theory. *Adv. Mater. Res.* **2009**, *79–82*, 1245–1248.
84. Zhou, X.; Shi, J.; Li, C. Effect of metal doping on electronic structure and visible light absorption of SrTiO₃ and NaTaO₃ (Metal = Mn, Fe, and Co). *J. Phys. Chem. C* **2011**, *115*, 8305–8311.
85. Kanhere, P.; Shenai, P.; Chakraborty, S.; Ahuja, R.; Zheng, J.; Chen, Z. Mono- and co-doped NaTaO₃ for visible light photocatalysis. *PCCP* **2014**, *16*, 16085–16094.
86. Wang, B.; Kanhere, P.; Chen, Z.; Nisar, J.; Pathak, B.; Ahuja, R. Anion-Doped NaTaO₃ for Visible Light Photocatalysis. *J. Phys. Chem. C* **2013**, *117*, 22518–22524.
87. Ni, L.; Tanabe, M.; Irie, H. A visible-light-induced overall water-splitting photocatalyst: conduction-band-controlled silver tantalate. *Chem. Commun.* **2013**, *49*, 10094–10096.
88. Li, M.; Zhang, J.; Dang, W.; Cushing, S.K.; Guo, D.; Wu, N.; Yin, P. Photocatalytic hydrogen generation enhanced by band gap narrowing and improved charge carrier mobility in AgTaO₃ by compensated co-doping. *PCCP* **2013**, *15*, 16220–16226.
89. Liu, J.W.; Chen, G.; Li, Z.H.; Zhang, Z.G. Hydrothermal synthesis and photocatalytic properties of ATaO₃ and ANbO₃ (A = Na and K). *Int. J. Hydrg. Energy* **2007**, *32*, 2269–2272.
90. Shi, H.; Li, X.; Iwai, H.; Zou, Z.; Ye, J. 2-Propanol photodegradation over nitrogen-doped NaNbO₃ powders under visible-light irradiation. *J. Phys. Chem. Solids* **2009**, *70*, 931–935.
91. Wang, R.; Zhu, Y.; Qiu, Y.; Leung, C.-F.; He, J.; Liu, G.; Lau, T.-C. Synthesis of nitrogen-doped KNbO₃ nanocubes with high photocatalytic activity for water splitting and degradation of organic pollutants under visible light. *Chem. Eng. J.* **2013**, *226*, 123–130.
92. Liu, G.; Ji, S.; Yin, L.; Xu, G.; Fei, G.; Ye, C. Visible-light-driven photocatalysts: (La/Bi + N)-codoped NaNbO₃ by first principles. *J. Appl. Phys.* **2011**, *109*, 063103.

93. Grinberg, I.; West, D.V.; Torres, M.; Gou, G.; Stein, D.M.; Wu, L.; Chen, G.; Gallo, E.M.; Akbashev, A.R.; Davies, P.K.; *et al.* Perovskite oxides for visible-light-absorbing ferroelectric and photovoltaic materials. *Nature* **2013**, *503*, 509–512.
94. Li, G.; Yan, S.; Wang, Z.; Wang, X.; Li, Z.; Ye, J.; Zou, Z. Synthesis and visible light photocatalytic property of polyhedron-shaped AgNbO_3 . *J. Chem. Soc. Dalton Trans.* **2009**, *40*, 8519–8524.
95. Li, G.; Kako, T.; Wang, D.; Zou, Z.; Ye, J. Enhanced photocatalytic activity of La-doped AgNbO_3 under visible light irradiation. *J. Chem. Soc. Dalton Trans.* **2009**, *13*, 2423–2427.
96. Konta, R.; Kato, H.; Kobayashi, H.; Kudo, A. Photophysical properties and photocatalytic activities under visible light irradiation of silver vanadates. *PCCP* **2003**, *5*, 3061–3065.
97. Xu, J.; Hu, C.; Xi, Y.; Wan, B.; Zhang, C.; Zhang, Y. Synthesis and visible light photocatalytic activity of $\beta\text{-AgVO}_3$ nanowires. *Solid State Sci.* **2012**, *14*, 535–539.
98. Sang, Y.; Kuai, L.; Chen, C.; Fang, Z.; Geng, B. Fabrication of a Visible-Light-Driven Plasmonic Photocatalyst of $\text{AgVO}_3@\text{AgBr}@\text{Ag}$ Nanobelt Heterostructures. *ACS App. Mater. Interfaces* **2014**, *6*, 5061–5068.
99. Ju, P.; Fan, H.; Zhang, B.; Shang, K.; Liu, T.; Ai, S.; Zhang, D. Enhanced photocatalytic activity of $\beta\text{-AgVO}_3$ nanowires loaded with Ag nanoparticles under visible light irradiation. *Sep. Purif. Technol.* **2013**, *109*, 107–110.
100. Joshi, U.A.; Palasyuk, A.M.; Maggard, P.A. Photoelectrochemical Investigation and Electronic Structure of a p-Type CuNbO_3 Photocathode. *J. Phys. Chem. C* **2011**, *115*, 13534–13539.
101. Lin, Y.; Yuan, G.; Sheehan, S.; Zhou, S.; Wang, D. Hematite-based solar water splitting: Challenges and opportunities. *Energy Environ. Sci.* **2011**, *4*, 4862–4869.
102. Parida, K.M.; Reddy, K.H.; Martha, S.; Das, D.P.; Biswal, N. Fabrication of nanocrystalline LaFeO_3 : An efficient sol-gel auto-combustion assisted visible light responsive photocatalyst for water decomposition. *Int. J. Hydrog. Energy* **2010**, *35*, 12161–12168.
103. Thirumalairajan, S.; Girija, K.; Hebalkar, N.Y.; Mangalaraj, D.; Viswanathan, C.; Ponpandian, N. Shape evolution of perovskite LaFeO_3 nanostructures: A systematic investigation of growth mechanism, properties and morphology dependent photocatalytic activities. *RSC Adv.* **2013**, *3*, 7549–7561.
104. Wei, Z.-X.; Wang, Y.; Liu, J.-P.; Xiao, C.-M.; Zeng, W.-W.; Ye, S.-B. Synthesis, magnetization, and photocatalytic activity of LaFeO_3 and $\text{LaFe}_{0.9}\text{Mn}_{0.1}\text{O}_{3-\delta}$. *J. Mater. Sci.* **2013**, *48*, 1117–1126.
105. Gao, F.; Chen, X.Y.; Yin, K.B.; Dong, S.; Ren, Z.F.; Yuan, F.; Yu, T.; Zou, Z.G.; Liu, J.M. Visible-Light Photocatalytic Properties of Weak Magnetic BiFeO_3 Nanoparticles. *Adv. Mater.* **2007**, *19*, 2889–2892.
106. Mohan, S.; Subramanian, B.; Bhaumik, I.; Gupta, P.K.; Jaisankar, S.N. Nanostructured $\text{Bi}_{(1-x)}\text{Gd}_x\text{FeO}_3$ —A multiferroic photocatalyst on its sunlight driven photocatalytic activity. *RSC Adv.* **2014**, *4*, 16871–16878.
107. Feng, Y.N.; Wang, H.C.; Luo, Y.D.; Shen, Y.; Lin, Y.H. Ferromagnetic and photocatalytic behaviors observed in Ca-doped BiFeO_3 nanofibres. *J. App. Phys.* **2013**, *113*, 146101.
108. Madhu, C.; Bellakki, M.B.; Manivannan, V. Synthesis and characterization of cation-doped BiFeO_3 materials for photocatalytic applications. *Indian J. Eng. Mater. Sci.* **2010**, *17*, 131–139.

109. Dhanasekaran, P.; Gupta, N.M. Factors affecting the production of H₂ by water splitting over a novel visible-light-driven photocatalyst GaFeO₃. *Int. J. Hydrot. Energy* **2012**, *37*, 4897–4907.
110. Tang, P.; Chen, H.; Cao, F.; Pan, G. Magnetically recoverable and visible-light-driven nanocrystalline YFeO₃ photocatalysts. *Catal. Sci. Technol.* **2011**, *1*, 1145–1148.
111. Yuan, Z.; Wang, Y.; Sun, Y.; Wang, J.; Bie, L.; Duan, Y. Sunlight-activated AlFeO₃/TiO₂ photocatalyst. *Sci. China Ser. B* **2006**, *49*, 67–74.
112. Takei, T.; Haramoto, R.; Dong, Q.; Kumada, N.; Yonesaki, Y.; Kinomura, N.; Mano, T.; Nishimoto, S.; Kameshima, Y.; Miyake, M. Photocatalytic activities of various pentavalent bismuthates under visible light irradiation. *J. Solid State Chem.* **2011**, *184*, 2017–2022.
113. Kako, T.; Zou, Z.; Katagiri, M.; Ye, J. Decomposition of Organic Compounds over NaBiO₃ under Visible Light Irradiation. *Chem. Mater.* **2006**, *19*, 198–202.
114. Chang, X.; Yu, G.; Huang, J.; Li, Z.; Zhu, S.; Yu, P.; Cheng, C.; Deng, S.; Ji, G. Enhancement of photocatalytic activity over NaBiO₃/BiOCl composite prepared by an in situ formation strategy. *Catal. Today* **2010**, *153*, 193–199.
115. Yu, X.; Zhou, J.; Wang, Z.; Cai, W. Preparation of visible light-responsive AgBiO₃ bactericide and its control effect on the *Microcystis aeruginosa*. *J. Photochem. Photobiol. B* **2010**, *101*, 265–270.
116. Sun, M.; Jiang, Y.; Li, F.; Xia, M.; Xue, B.; Liu, D. Dye degradation activity and stability of perovskite-type LaCoO_{3-x} ($x = 0\text{--}0.075$). *Mater. Trans.* **2010**, *51*, 2208–2214.
117. Tang, P.; Sun, H.; Cao, F.; Yang, J.; Ni, S.; Chen, H. Visible-light driven LaNiO₃ nanosized photocatalysts prepared by a sol-gel process. *Adv. Mater. Res.* **2011**, *279*, 83–87.
118. Li, J.; Zeng, J.; Jia, L.; Fang, W. Investigations on the effect of Cu²⁺/Cu¹⁺ redox couples and oxygen vacancies on photocatalytic activity of treated LaNi_{1-x}Cu_xO₃ ($x=0.1, 0.4, 0.5$). *Int. J. Hydrot. Energy* **2010**, *35*, 12733–12740.
119. Singh, J.; Uma, S. Efficient Photocatalytic Degradation of Organic Compounds by Ilmenite AgSbO₃ under Visible and UV Light Irradiation. *J. Phys. Chem. C* **2009**, *113*, 12483–12488.
120. Shi, J.; Ye, J.; Zhou, Z.; Li, M.; Guo, L. Hydrothermal Synthesis of Na_{0.5}La_{0.5}TiO₃–LaCrO₃ Solid-Solution Single-Crystal Nanocubes for Visible-Light-Driven Photocatalytic H₂ Evolution. *Chem. Eur. J.* **2011**, *17*, 7858–7867.
121. Borse, P.H.; Cho, C.R.; Yu, S.M.; Yoon, J.H.; Hong, T.E.; Bae, J.S.; Jeong, E.D.; Kim, H.G. Improved photolysis of water from ti incorporated double perovskite Sr₂FeNbO₆ lattice. *Bull. Korean Chem. Soc.* **2012**, *33*, 3407–3412.
122. Borse, P.H.; Lim, K.T.; Yoon, J.H.; Bae, J.S.; Ha, M.G.; Chung, E.H.; Jeong, E.D.; Kim, H.G. Investigation of the physico-chemical properties of Sr₂FeNb_{1-x}W_xO₆ ($0.0 \leq x \leq 0.1$) for visible-light photocatalytic water-splitting applications. *J. Korean Phys. Soc.* **2014**, *64*, 295–300.
123. Hu, R.; Li, C.; Wang, X.; Sun, Y.; Jia, H.; Su, H.; Zhang, Y. Photocatalytic activities of LaFeO₃ and La₂FeTiO₆ in p-chlorophenol degradation under visible light. *Catal. Commun.* **2012**, *29*, 35–39.
124. Hatakeyama, T.; Takeda, S.; Ishikawa, F.; Ohmura, A.; Nakayama, A.; Yamada, Y.; Matsushita, A.; Yea, J. Photocatalytic activities of Ba₂RBiO₆ (R = La, Ce, Nd, Sm, Eu, Gd, Dy) under visible light irradiation. *J. Ceram. Soc. Jpn.* **2010**, *118*, 91–95.

125. Clark, J.H.; Dyer, M.S.; Palgrave, R.G.; Ireland, C.P.; Darwent, J.R.; Claridge, J.B.; Rosseinsky, M.J. Visible light photo-oxidation of model pollutants using $\text{CaCu}_3\text{Ti}_4\text{O}_{12}$: An experimental and theoretical study of optical properties, electronic structure, and selectivity. *J. Am. Chem. Soc.* **2011**, *133*, 1016–1032.
126. Iwakura, H.; Einaga, H.; Teraoka, Y. Photocatalytic Properties of Ordered Double Perovskite Oxides. *J. Novel Carbon Resour. Sci.* **2011**, *3*, 1–5.
127. Zhu, S.; Fu, H.; Zhang, S.; Zhang, L.; Zhu, Y. Two-step synthesis of a novel visible-light-driven $\text{K}_2\text{Ta}_2\text{O}_{6-x}\text{N}_x$ catalyst for the pollutant decomposition. *J. Photochem. Photobiol. A* **2008**, *193*, 33–41.
128. Kanhere, P.; Tang, Y.; Zheng, J.; Chen, Z. Synthesis, photophysical properties, and photocatalytic applications of Bi doped NaTaO_3 and Bi doped $\text{Na}_2\text{Ta}_2\text{O}_6$ nanoparticles. *J. Phys. Chem. Solids* **2013**, *74*, 1708–1713.
129. Hara, M.T.T.; Kondo, J.N.; Domen, K. Photocatalytic reduction of water by TaON under visible light irradiation. *Catal. Today* **2004**, *90*, 313–317.
130. Ishikawa, A.; Takata, T.; Kondo, J.N.; Hara, M.; Kobayashi, H.; Domen, K. Oxysulfide $\text{Sm}_2\text{Ti}_2\text{S}_2\text{O}_5$ as a Stable Photocatalyst for Water Oxidation and Reduction under Visible Light Irradiation ($\lambda \leq 650$ nm). *J. Am. Chem. Soc.* **2002**, *124*, 13547–13553.
131. Siritanaratkul, B.; Maeda, K.; Hisatomi, T.; Domen, K. Synthesis and Photocatalytic Activity of Perovskite Niobium Oxynitrides with Wide Visible-Light Absorption Bands. *ChemSusChem* **2011**, *4*, 74–78.
132. Maeda, K.; Higashi, M.; Siritanaratkul, B.; Abe, R.; Domen, K. SrNbO_2N as a Water-Splitting Photoanode with a Wide Visible-Light Absorption Band. *J. Am. Chem. Soc.* **2011**, *133*, 12334–12337.
133. Higashi, M.; Abe, R.; Takata, T.; Domen, K. Photocatalytic Overall Water Splitting under Visible Light Using ATaO_2N ($\text{A} = \text{Ca}, \text{Sr}, \text{Ba}$) and WO_3 in a IO_3^-/I^- Shuttle Redox Mediated System. *Chem. Mater.* **2009**, *21*, 1543–1549.
134. Maeda, K.; Domen, K. Preparation of $\text{BaZrO}_3-\text{BaTaO}_2\text{N}$ solid solutions and the photocatalytic activities for water reduction and oxidation under visible light. *J. Catal.* **2014**, *310*, 67–74.
135. Le Paven-Thivet, C.; Ishikawa, A.; Ziani, A.; Le Gendre, L.; Yoshida, M.; Kubota, J.; Tessier, F.; Domen, K. Photoelectrochemical Properties of Crystalline Perovskite Lanthanum Titanium Oxynitride Films under Visible Light. *J. Phys. Chem. C* **2009**, *113*, 6156–6162.
136. Kako, T.; Kikugawa, N.; Ye, J. Photocatalytic activities of AgSbO_3 under visible light irradiation. *Catal. Today* **2008**, *131*, 197–202.